



Lawrence Berkeley Laboratory

UNIVERSITY OF CALIFORNIA

Materials & Chemical Sciences Division

National Center for Electron Microscopy

Submitted to Acta Metallurgica

Improvement in Intrinsic Coercivity of Sintered Fe-Nd-B Magnets by the Introduction of Non-Magnetic Dispersoids

R. Ramesh, G. Thomas, and B.M. Ma

July 1988

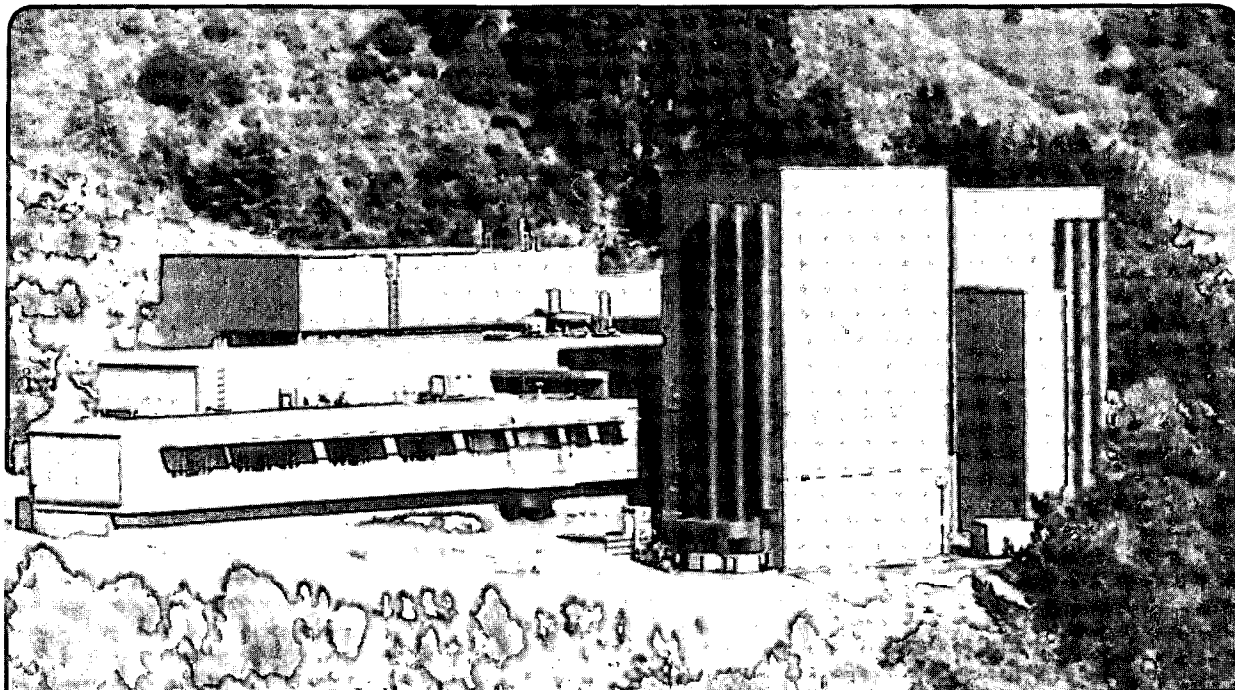
LAWRENCE
BERKELEY LABORATORY

SEP 30 1988

LIBRARY AND
DOCUMENTS SECTION

For Reference

Not to be taken from this room



LBL-25648
c.1

DISCLAIMER

This document was prepared as an account of work sponsored by the United States Government. While this document is believed to contain correct information, neither the United States Government nor any agency thereof, nor the Regents of the University of California, nor any of their employees, makes any warranty, express or implied, or assumes any legal responsibility for the accuracy, completeness, or usefulness of any information, apparatus, product, or process disclosed, or represents that its use would not infringe privately owned rights. Reference herein to any specific commercial product, process, or service by its trade name, trademark, manufacturer, or otherwise, does not necessarily constitute or imply its endorsement, recommendation, or favoring by the United States Government or any agency thereof, or the Regents of the University of California. The views and opinions of authors expressed herein do not necessarily state or reflect those of the United States Government or any agency thereof or the Regents of the University of California.

IMPROVEMENT IN INTRINSIC COERCIVITY OF SINTERED Fe-Nd-B MAGNETS BY
THE INTRODUCTION OF NON-MAGNETIC DISPERSOIDS

R.Ramesh and G.Thomas

Department of Materials Science and Mineral Engineering and National
Center for Electron Microscopy, Materials and Chemical Sciences Division,
Lawrence Berkeley Laboratory, University of California, Berkeley CA
94720.

B.M.Ma

Department of Metallurgical Engineering and Materials Science
Wean Hall, Carnegie-Mellon University,
Pittsburgh, PA 15213.

ABSTRACT : The microstructure of Ho-substituted sintered Fe-Nd-B magnets, prepared by two different routes, has been characterized in order to understand the changes in intrinsic coercivity with Ho content. Spherical inclusions in the size range of 500Å-1µm have been observed inside the matrix $\text{Re}_2\text{Fe}_{14}\text{B}$ grains. Characterization by xray diffraction, electron microdiffraction and energy dispersive xray microanalysis, shows that these inclusions are fcc rare earth oxides. The volume fraction of these inclusions increases with Ho content. Ho partitions preferentially into the matrix phase and no segregation of Ho to the interphase interfaces is observed. Lorentz electron microscopy experiments suggest that the inclusions in the lower end of the size distribution are capable of pinning the magnetic domain walls and hence these non-magnetic inclusions must contribute to the increase in intrinsic coercivity.

INTRODUCTION:

During the course of a systematic evaluation of the effect of quaternary rare earth additions upon the microstructure and magnetic properties of Fe-Nd-B magnets, abnormally high values of intrinsic coercivity were observed in the case of Holmium additions, although the anisotropy field of $\text{Ho}_2\text{Fe}_{14}\text{B}$ (79kOe at room temperature compared to $\text{Nd}_2\text{Fe}_{14}\text{B}$ which is 71kOe) dictates that the intrinsic coercivity will not change significantly with Ho addition. Thus a detailed analysis of the microstructure and magnetic properties of various Ho-substituted alloys was undertaken to understand the origin of the high intrinsic coercivities.

The effects of several quaternary rare earth additions are being investigated in order to overcome two main problems associated with the ternary Fe-Nd-B magnets. These problems are¹: (1) the high value of the temperature coefficient of saturation magnetization, dM_s/dT and, (2) the high value of the temperature coefficient of the intrinsic coercivity, $d(iH_c)/dT$. The cause for concern is due to the low Curie temperature of $\text{Nd}_2\text{Fe}_{14}\text{B}$ ², which produces a high reversible temperature coefficient of remanence. In addition, the rapid fall of intrinsic coercivity, iH_c , with temperature means that normally encountered demagnetizing fields can produce large irreversible losses of magnetization. Dy and Tb (either in the elemental form or as the oxide) have been the most useful alloying additions in substantially overcoming the high temperature coefficient of iH_c ³⁻⁹. Both of them increase the anisotropy field of the $\text{RE}_2\text{Fe}_{14}\text{B}$ phase thus raising the iH_c through the dependence of iH_c on the anisotropy field. In a recent analytical electron microscopic study¹⁰, it was shown that in Fe-Nd-Dy-B magnets, Dy partitions almost completely into the matrix $\text{RE}_2\text{Fe}_{14}\text{B}$ phase when Dy is added in the casting stage. The increase in the magnetocrystalline anisotropy field of the $\text{RE}_2\text{Fe}_{14}\text{B}$ phase due to the substitution of Nd by Dy was shown to be directly responsible for the increase in iH_c of Dy substituted magnets. For certain special military applications which require full compensation of the reversible temperature coefficient of saturation magnetization, addition of Holmium has been found to be useful¹¹. Ma et.al¹¹ have examined the temperature dependent magnetization of many alloyed Fe-Nd-B magnets based on computer calculations. Although no data about the microstructure of these magnets and how it influences the magnetic properties, especially the intrinsic coercivity, iH_c , the energy product, $(BH)_{\text{max}}$ and the remanence have been reported, it was shown that for an alloy in which 35% of the Nd was substituted by Ho the iH_c was 16.45kOe. This value is higher than the

normal iH_c of an Fe-Nd-B magnet which is about 13kOe. Since the anisotropy field of $Ho_2Fe_{14}B$ is 79kOe as compared to 71kOe for $Nd_2Fe_{14}B$ ¹²⁻¹⁵ it is unlikely that the change in the iH_c could be caused merely by an increase in the effective anisotropy field of the $RE_2Fe_{14}B$ phase, as observed in the case of Dy additions to Fe-Nd-B magnets¹⁰. Thus microstructural changes could be occurring which could effect the increase in iH_c . Hence, a systematic study of the effect of Ho additions upon the microstructure and magnetic properties of ternary Fe-Nd-B magnets was thought to be essential. Such results are of importance, not only in understanding the effect of quaternary rare earth additions on the magnetic properties, but also in systematically characterizing the structural, microstructural and microanalytical changes which may be occurring due to the additions. Since the final microstructure and magnetic properties depend to a large extent on the processing conditions employed, careful analysis of the microstructure has to be carried out to identify the changes due to the changes in processing.

EXPERIMENTAL:

(1) **Alloys** : Quaternary Fe-Nd-Ho-B alloys with varying amounts of Ho were made by two different processing routes. In the first method, a master alloy of composition 2.32wt.%Nd-26.83wt.%Ho-1wt.5 B-balance Fe was blended with a sintering aid of composition 42wt.% Nd-1wt.% B-balance Fe . These alloys were prepared by vacuum induction melting. The ingots were crushed, pulverized and jet milled to an average particle size of a few microns. The desired alloy composition was obtained by blending the master alloy with the sintering aid. The powder was then aligned in a magnetic field of 40kOe and cold isostatically pressed. The magnets were sintered at 1060°C for 3 hours under vacuum. Post-sintering aging was carried out at 550°C for 3 hours to obtain the optimum coercivity. The alloy compositions and magnetic properties are presented in Table I.

In the second method the desired alloy composition of 12 wt.% Ho-23 wt.% Nd-1 wt.% B-balance Fe was prepared by induction melting the pure elements. The ingot was crushed , pulverized and jet milled to an average particle size of 3-4 microns. The powders were then processed identically as the magnets prepared in the first method.

(2) **Magnetic Measurements** : All magnets were pulse magnetized in a

field of 40kOe prior to measurement. Magnetic properties were measured using a hysteresigraph at a maximum applied field of 25kOe.

(3) **Structural and Microstructural characterization** : Xray diffraction was carried using a Siemens D-500 diffractometer on polished samples, using Cu K_{α} radiation. Samples for Transmission Electron Microscopy (TEM) were prepared by cutting 500 micrometer slices from the bulk magnet, mechanically grinding them to a thickness of 50 micrometers, followed by Argon ion milling. Ion milling was carried out in a liquid nitrogen stage at 6kV with a gun current of 0.3mA, corresponding to a specimen current of 30-40 microamperes. TEM was carried out using a Philips 400 TEM/STEM at 100 kV. Analytical Electron Microscopy(AEM) was accomplished on a JEOL 200CX at 200 kV. This microscope is fitted with both a Be window Energy Dispersive Xray (EDX) detector as well as an ultra-thin window EDX detector. The ultra-thin window detector enables the detection and quantification of elements upto boron. Care was taken to ensure statistical significance of the xray data by acquiring at least 10^5 counts. Spectral deconvolution and quantification was carried out using the Kevex 8000 system software using theoretically generated thin foil k-factors. In the case of oxygen, the corrected value of the k-factors was employed. Microanalysis line profiles were carried out at various regions in many samples in order to check the correctness of the profiles as well as the validity and reliability of the microanalytical data. Lorentz Electron Microscopy (LEM) was used to examine the interaction of the domain walls with the microstructural features. This was carried out using a Hitachi HU 650 TEM at 500kV . The goniometer tilting stage was used to move the domain walls in order to study the interaction of the domain walls with the microstructural features dynamically.

RESULTS :

(1) **Magnetic Properties** : Figs.1(a-c) show the remanence, B_r , intrinsic coercivity, iH_c , and energy product, $(BH)_{max}$, respectively as a function of Ho content in the alloys processed by the first processing route, i.e., blending of the master alloy with the sintering aid. For comparison, the corresponding magnetic properties of the sample prepared by the second method, i.e., in which Ho was added to the alloy in the induction melting stage, are also shown in these figures. The intrinsic coercivity rises almost linearly with weight % of Ho in the alloy. This result is surprising since the anisotropy field of $Ho_2Fe_{14}B$ is 79 kOe while that of $Nd_2Fe_{14}B$ is

71 kOe. Thus a mere substitution of Nd by Ho should not lead to such a large change in the iH_c . This is authenticated by the iH_c of the magnet which was processed by the second method, i.e, in which Ho was added to the alloy in the vacuum induction melting stage. In this case, as shown in Table I, the iH_c is only 11.4 kOe as compared to that of a sample with the same amount of Ho, but processed by the first method. In this case the iH_c is 20.5 kOe, under identical measurement conditions. The second quadrant of the hysteresis loops of samples (1-5) is shown in Figs.2(a&b). In samples (1)-(4) as the Ho content is progressively increasing, the loops become less square and in the case of the 12 wt.% sample(4), a definite kink appears in the B-H loop. The magnetization starts to drop at -9kOe but the iH_c value is -20.5 kOe ! The shape of the hysteresis loops and the iH_c values were obtained repeatably, thus removing any doubt that the measurement could be in error. Due to the surprising nature of the iH_c data (and to be sure), the hysteresis loops were generated on a different hysteresigraph and identical results were obtained. The reliability of the iH_c values was verified by this duplicate measurement. The temperature dependence of iH_c and Br is shown in the hysteresis loops in Fig.3(a &b) for sample (3) and (5) respectively. The kink in sample (3) remains at 150°C also and the iH_c also remains higher than that of sample(5).

Structural and Microstructural Characterization : Figs.4 (a-e) show xray diffractograms of samples 1-5 respectively. The main peaks can be indexed as arising from the matrix $RE_2Fe_{14}B$ phase. However, there are two peaks in the xray diffractograms of samples (1-4) which do not exist in that of sample 5. In the diffractograms 1-4, a minor peak can be observed for 2θ values of about $35-36^\circ$. This peak is not found in sample 5 at all. Similarly, a minor peak is found in samples (1-4) at 2θ values of about 53° , which is not found in sample (5). The peak at 36° corresponds to a d-spacing of 2.5357\AA , while the peak at 53° corresponds to a d-spacing of 1.7940\AA . The highest intensity peak at 45° corresponds to the (006) reflection of the $RE_2Fe_{14}B$ phase, due to the alignment of the c-axis along the axis of the cylindrical sample. The ratio of integrated intensity of the peak at 36° and at 53° , to that of the (006) matrix reflection is given in Table II for all the samples. It is clearly seen that the ratio increases from sample (1) to (4) and is zero for sample (5). This indicates that a new phase is present in samples (1-4), which is not present in sample (5). This will be elaborated further through the results of TEM studies.

In order to identify the structure and composition of the new phase(s) present in samples (1-4), TEM was carried out on all samples. Specifically, samples (4) and (5) were examined in detail, since these two samples had the same nominal composition but exhibited a large difference in iHc. Electron microscopic investigations revealed that the overall microstructure in both sample (4) and (5) was the same. It consists of large (about 5-10 micrometers) grains of the matrix $RE_2Fe_{14}B$ phase, at the triple junctions of which an fcc phase is observed. The details of the microstructural aspects are discussed in earlier papers¹⁶⁻²¹. However, the major difference was that in the case of sample (4), several inclusions were observed inside the matrix grains. Fig. 5 shows typical examples of these inclusions. These inclusions varied in size from about 500Å to about 5000Å and were generally rounded. Such inclusions were observed in samples (1-3) also. More of the inclusions observed were in the lower end of the size range, although a quantitative estimation was not possible. However, it was evident that the density of the inclusions increased monotonically from sample (1) to (4) and they were not observed in sample (5) at all. This matches well with the observation that the xray peak ratios increased monotonically from sample (1) to (4) and was zero for sample (5). Although many of the particles had amorphised due to ion beam damage (during Argon ion milling), it was possible to find one particle that was crystalline. Fig. 6(a, (b) and (c) respectively show the microdiffraction patterns, from the large particle in Fig.5, in the [110], [112] and [013] zone axis orientations of a fcc structure. The lattice parameter measured from the diffraction patterns was 5.12Å, which agreed well with the xray diffraction data.

Microanalysis: Microanalysis was carried out to determine the composition of the inclusions as well as determine the partitioning of Ho between the matrix and the grain boundary phase, both in the samples with inclusions and without inclusions. In earlier papers^{20,21} it has been shown that the possible segregation of a substituent species, such as Dy or Al, to the interphase interfaces could be a potential mechanism for improving the intrinsic coercivity of nucleation controlled magnets such as sintered Fe-Nd-B. In such magnets, magnetization reversal occurs by the nucleation of domain walls at defects such as interphase interfaces, grain boundaries, etc., at which the local magnetocrystalline anisotropy is much lower than that in the bulk of the sample. Fig.7(a) is a bright field micrograph showing the grain boundary phase at the triple junctions. This figure also shows the line profiling across the grain boundary phase, to

detect possible segregation at the two-phase interfaces. Fig.7(b) shows a typical EDX spectrum from the grain boundary fcc phase. As was shown in earlier papers, the fcc phase is rich in Nd and is stabilized by the presence of oxygen. Fig.7(c) shows a typical EDX line profile across the grain boundary phase from sample No.4, shown in Fig.7(a). Since this was obtained using a Be window EDX detector, oxygen is not detected. This profile shows that the grain boundary phase is depleted in Ho (about 0.6 atomic %) while the matrix contains about 4.5 atomic % of Ho. Similar results were obtained from sample No.5 also, as well as in the other samples. Thus, it was clear that Ho partitioned preferentially into the matrix phase, within the limits of the experimental errors. Also, this indicated that no significant segregation or depletion of Ho was occurring at the fcc phase-matrix interfaces, in the case of all the samples. Using a focussed probe of diameter 400Å, it was possible to obtain an EDX spectrum from the inclusion. Fig.7(d) shows a typical EDX spectrum from an inclusion. This indicates that the inclusion is rich in oxygen and Ho. The quantified composition data for the different microstructural regions is summarized in Table III. The microanalytical data along with the diffraction information that the inclusion has an fcc structure, means that the inclusions are rare earth oxide particles. Examination of data on the oxides of rare earths reveals the presence of an fcc oxide with the NaCl structure, with a lattice parameter of 5.07Å. This agrees well with the xray diffraction data where the peaks corresponding to d-spacings of 2.5357Å and 1.7940Å correspond to the (200) and (220) reflections from a fcc structure with lattice parameter of 5.07Å. Thus, it was clear that the inclusions were fcc rare earth oxides.

The presence of the inclusions inside the matrix $RE_2Fe_{14}B$ phase and the observation of kinks in the second quadrant of the hysteresis loops, Fig.2(a), suggested that domain wall pinning may be occurring at the inclusions. With this in mind, the interaction of domain walls with the inclusions was examined by Lorentz microscopy. Again, since sample No.4 exhibited the largest density of the inclusions and the highest iH_c , this sample was examined.

Lorentz Electron Microscopy: The samples examined had the c-axis in the plane of the foil, thus making it possible to move the domain walls by tilting the foil, thereby changing the in-plane component of the objective lens magnetic field. In this experiment, the interaction of the moving domain walls with particles in the size range 300-500Å was examined, since this size range is within an order of magnitude of the domain wall

width, which is typically about 50\AA in Nd-Fe-B magnets. Fig.8(a) is a bright field image of a typical inclusion about which the tilting experiments were carried out. In Fig.8(b-d) the Lorentz images in the Fresnel mode show various positions of the domain wall as a function of foil tilt angle. The strong interaction of the domain wall with the inclusion is evident in the image in Fig.8(d), where the wall is sharply bent near the inclusion (indicated by arrows) and is stuck to the inclusion. In this case, further movement of the domain wall from this pinned configuration required large tilt angles. Very often, spike domains were observed when the wall was pinned strongly to the inclusion. One example is shown in Fig.9(a -c), in which the wall was moved until it was pinned at the inclusion. The bright field image shows the inclusion (about 500\AA diameter), while the under-focussed and over-focussed Fresnel images in Fig.9(b&c) show the pinned configuration, with the formation of a spiked domain wall. In this case also, further movement of the wall required large angles of tilting. In the case of large inclusions, as in Fig.10 (about 1.0 micron), several domain walls were observed around each inclusion. In this case, the domain walls moved very easily across the inclusions.

DISCUSSION:

(1) **Structure and Microstructure :** The xray diffraction data along with the microdiffraction and AEM data clearly elucidate the structure and composition of the inclusions observed in samples (1-4). That these inclusions are related to the processing steps is also clear, since the inclusions are not observed in sample No.5, in which Ho was added in the casting stage itself. The microdiffraction data confirms the xray diffraction inference that the inclusions are face centred cubic, with a lattice parameter of 5.07\AA . The AEM data conclusively reveals the presence of oxygen and holmium in the inclusion, thus indicating that the inclusions are (Nd-Ho)oxide. The distribution of the oxide inclusions appears to be random, although more small inclusions were observed compared to large inclusions. The rounded shape of the inclusions and the absence of any specific orientation relationship indicates that they did not form by a solid state precipitation process.

(2) **Microstructure - Magnetic Property Correlation :**

The decrease in remanence with Ho addition can be attributed to two causes : (1) the replacement of Nd by Ho leads to anti-ferromagnetic coupling of the Ho spins to the Fe spins ; (2) the Nd-Ho oxide inclusions, which are paramagnetic at room temperature. However, the increase in

intrinsic coercivity with Ho content in samples (1-4) cannot be explained by a simple increase in the effective anisotropy field of the $\text{RE}_2\text{Fe}_{14}\text{B}$ phase, since the anisotropy field of $\text{Ho}_2\text{Fe}_{14}\text{B}$ is not very different from that of $\text{Nd}_2\text{Fe}_{14}\text{B}$. Thus, assuming (to a first approximation) a rule of mixtures, the effective anisotropy field when 4.5 at.% Ho replaces Nd should be 74.5 kOe, based on anisotropy field values of 71 kOe for $\text{Nd}_2\text{Fe}_{14}\text{B}$ and 79 kOe for $\text{Ho}_2\text{Fe}_{14}\text{B}$. This is the case for samples (4) and (5). However, the iH_c for sample (4) is 20.5 kOe while for sample (5) it is only 11.4 kOe. Hirosawa et. al²² have shown that the nucleation field, made up of the sum of the intrinsic coercivity and the effective demagnetizing field, I_S ($I_S = 4\pi M_S$), is linearly related to the effective anisotropy field of the $\text{RE}_2\text{Fe}_{14}\text{B}$ phase. Thus, $(iH_c + I_S) = c \cdot H_A$, where H_A is the effective anisotropy field. In this case, "c" is the slope of the linear fit and was found to be 0.38. In Fig.11, the nucleation field, defined by the above relationship, is plotted against the effective anisotropy field. A linear fit is obtained, but the slope is much larger than 0.38. The fact that the intrinsic coercivity is increasing at a rate faster than that at which the effective anisotropy field is, means that the effective anisotropy field is not the most important factor affecting the intrinsic coercivity. Thus, it appears that the magnetization reversal and intrinsic coercivity of samples (1-4) may not be classified as due to a typical "nucleation type"²³ magnet, unlike in the case of sample (5). Hence, some domain wall pinning in the bulk of the magnet needs to be invoked to explain the higher intrinsic coercivity values as well as the kinked second quadrant loops, especially in samples (2,3 and 4). This is more so since microanalysis of the matrix-fcc phase interface as well as the grain boundaries, which are two of the most potent domain wall nucleation sites in Fe-Nd-B magnets, indicates no difference in samples (4) and (5). The absence of any micro-segregation near the interphase interfaces also rules out the possibility of any local increase in the effective anisotropy field, thus leading to a higher nucleation field.

The kinks in the second quadrant of the B-H loops suggest that domain wall motion is prevented after the initial nucleation step, thus delaying further reversal of the grain in question. Indeed, evidence for domain wall pinning has been found by Lorentz microscopy studies, wherein, particles in the lower end of the size spectrum do prevent the motion of domain wall to a significant extent. However, this information should be considered qualitative, since the exact field conditions in the sample cannot be determined. In addition, the two-dimensional nature of the TEM foils, even

in a high voltage microscope, is likely to induce effects which may not have an equivalent in bulk magnets. However, along with the experimental observation of high iH_c values as well as kinked second quadrant B-H loops, in samples 2,3 and especially 4, the Lorentz microscopy observations have enhanced credibility. These results, along with the structural and microstructural information that samples (1-4) contain Nd-Ho oxide inclusions, mean that the non-magnetic oxide particles may be pinning the domain walls, leading to higher iH_c values as compared to sample (5).

Parker et.al^{22,23} have examined the influence of Nb on the magnetic properties of Nd/Dy-Fe-B magnets and have observed 200-500Å Nb-rich particles inside the $RE_2Fe_{14}B$ grains, which act as pinning sites for domain walls. These observations lend support to the experimental observations made in this study. The wide range of inclusion sizes, observed in this study, however, precludes theoretical estimation of the contribution of domain wall pinning to the iH_c observed. Thus, experiments with additions of particles of controlled size and size distribution, as well as different magnetic properties, need to be carried out to fully understand the contribution of domain wall pinning in the bulk of the magnet, to the overall iH_c of the magnet. The results presented here could have significant implications in terms of the potential range of applications of these magnets. For example, upon comparing the properties of sample(3) and (5), it is seen that about 50% increase in the iH_c can be obtained along with a higher remanence and energy product, simply by changing the form in which Ho is added to the alloy. Indeed, it should be possible to achieve similar improvements in the iH_c by introducing other magnetic/non-magnetic inclusions of suitable size into the matrix $RE_2Fe_{14}B$ phase. Such experiments are in progress.

CONCLUSIONS: The microstructure of Ho-substituted Fe-Nd-B magnets prepared by two different routes has been characterized in order to understand the increase in iH_c with Ho content in samples prepared by blending of two master alloys. In addition to the general microstructure, described in detail in earlier papers¹⁶⁻¹⁹, through xray diffraction and electron microscopy techniques inclusions with fcc structure have been observed inside the matrix $RE_2Fe_{14}B$ phase. The volume fraction of the inclusions increases with Ho content, as inferred from the increase in the $(200)_{fcc}$ and $(220)_{fcc}$ xray peaks in samples (1-4), with Ho content, as well as from the electron microscopy observations. Through analytical

electron microscopy, the inclusions have been determined to be Nd-Ho oxide. The inclusions have been observed in a size spectrum ranging from 300Å to 6000Å, with more of the inclusions in the lower end of the size spectrum. Lorentz microscopy suggests domain wall pinning at the smaller inclusions, especially those within 600Å diameter. The observation of pinning is consistent with the observation of kinks in the second quadrant of the hysteresis loops, in the case of samples with inclusions. Since the anisotropy field of $\text{Ho}_2\text{Fe}_{14}\text{B}$ is almost the same as that of $\text{Nd}_2\text{Fe}_{14}\text{B}$, the increase in iH_c with Ho content cannot be explained as being caused by an increase in the effective anisotropy field of the $\text{RE}_2\text{Fe}_{14}\text{B}$ phase. Increase in iH_c due to micro-segregation of Ho can also be ruled out since the micro-analytical data indicates no segregation of Ho to grain boundaries or matrix-fcc phase interfaces. Hence, it is suggested that domain wall pinning in the bulk of the magnet, at the inclusions, is responsible, at least in part, for the increase in iH_c observed with Ho additions, in samples (1-4). This inference is supported by a monotonic increase in the relative intensity of the $(200)_{\text{fcc}}$ and $(220)_{\text{fcc}}$ peaks with Ho content, concurrent with the increase in iH_c . Finally, it is suggested that in order to overcome the difficulties due to the size spectrum of the inclusions, systematic experiments, with additions of particles of controlled size and distribution, need to be carried out to fully understand the role of domain wall pinning in the bulk of the magnet by fine non-magnetic inclusions.

ACKNOWLEDGEMENTS : The authors wish to acknowledge the technical assistance of Mr. C.J.Echer of the National Center for Electron Microscopy, Lawrence Berkeley Laboratory. This work was supported by the Director, Office of Energy Research, Office of Basic Energy Sciences, Materials Science Division of the U.S.Department of Energy under contract No. DE-AC03-76SF00098.

REFERENCES

1. J.D.Livingston, in Proc. of ASM Symposium on Soft and Hard Magnetic Materials, Ed. J.A.Salsgiver et.al, 71-79(1986), Florida.
2. M.Sagawa, S.Fujimura, M.Togawa, H.Yamamoto and Y.Matsuura, J. Appl. Phys.55, 2083(1984).
3. M.Sagawa, S.Fujimura, H.Yamamoto, Y.Matsuura and K.Hiraga, IEEE Trans. Magnetics,Mag-21, 1584(1984).
4. M.Tokunaga, N.Meguro, M.Endoh, S.Tanigawa and H.Harada, IEEE Trans. Magnetics, Mag-21, 1964(1985).
5. W.Li, L.Jiang, D.Wang, T.Sun and J.Zhu, J.of Less Common Metals, 126,95(1986).
6. H.Fujii, W.E.Wallace and E.B.Boltich, J.Magnetism and Magnetic Materials, 61, 251(1986).
7. W.Rodewald, J.Less Common Metals, 111, 77(1985).
8. M.H.Ghandehari, Appl.Phys. Lett.48, 548(1986).
9. M.Tokunaga, M.Tobise, N.Meguro and H.Harada, IEEE Trans. on Magn., MAG-22, 904(1986).
10. R.Ramesh, G.Thomas and B.M.Ma, Proc. MRS Symposium on Permanent Magnetic Materials, MRS Spring Meeting, Anaheim, California, April 1987.
11. B.M.Ma, K.S.V.L.Narasimhan and J.C.Hurt, IEEE Trans. Magnetics, Mag-22, 1081(1986).
12. E.B.Boltich, E.Oswald, M.Q.Huang, S.Hirosawa and W.E.Wallace, J. Appl. Phys.57, 4106(1985).
13. J.M.D.Coey, J.Less Common Metals, 126, 21(1986).
14. C. Abache and H.Oesterreicher, J.Appl. Phys., 57, 4112(1985).
15. R.Grossinger, X.K.Sun, R.Eibler, K.H.J.Buschow and H.R.Kirchmayr, J. Magnetism and Magnetic Materials, 58, 55(1986).
16. R.Ramesh, K.M.Krishnan, E.Goo, G.Thomas, M.Okada and M.Homma, J. Magnetism and Magnetic Materials, 54-57, 563(1986).
17. R.Ramesh, J.K.Chen and G.Thomas, J.Appl. Phys., 61, 2993(1987).
18. R.K.Mishra, J.K.Chen and G.Thomas, J Appl. Phys.,59, 2244(1986).
19. R.Ramesh, G.Thomas, M.Okada and M.Homma, Paper No.AC-07, Intermag 1987, Tokyo, Japan.
20. R.Ramesh, J.K.Chen, L.K.Rabenberg and G.Thomas, in Proc. ASM Symp. on Hard and Soft Magnetic Materials, Eds. J.A.Salsgiver, K.S.V.L.Narasimhan, P.K.Rastogi, A.R.Traut, D.J.Bailey and H.R.Sheppard, Cincinnati, Ohio, 10-15 Oct., 1987, pp1-26, Published by ASM.

21. R.Ramesh, G.Thomas and B.M.Ma, in Proc. of MRS Symp. on Microstructure-Property Correlations in Magnetic Materials, Symposium L, May 30-June 3, 1988, Tokyo, Japan.
22. S.Hirosawa, K.Tokuhara, Y.Matsuura, H.Yamamoto, S.Fujimura and M.Sagawa, JI. of Magn. and Mag. Matls., 61,363(1986).
23. J.D.Livingston, Paper No.AC-06, Intermag 1987, Tokyo, Japan.
24. S.F.H.Parker, P.J.Grundy and J.Fidler, J. Magnetism and Magnetic Materials, 66, 74(1987).
25. S.F.H.Parker,R.Pollard, D.G.Lord and P.J.Grundy, Paper No.AC-03, Intermag 1987, Tokyo, Japan.

FIGURE CAPTIONS

- Figure 1 : Effect of Ho additions on (a) the remanence, B_r ; (b) intrinsic coercivity, iH_c and (c) energy product, $(BH)_{max}$ of Fe-Nd-B magnets, processed by blending of two master alloys. The corresponding magnetic properties of sample (5) are also shown for comparison.
- Figure 2 : (a) Room temperature second quadrant hysteresis loops of samples (1-4) at a maximum applied field of 25kG. Note the kink in the loops for samples (1-4), especially sample (4) ; (b) same plot for sample (5). Note the much lower iH_c of sample(5) compared to sample (4) although both have the same nominal composition.
- Figure 3 : (a) Second quadrant hysteresis loops of sample (3) at different temperatures. Note the persistence of kinks at 150°C also ; (b) Second quadrant hysteresis loops of sample (5) at different temperatures.
- Figure 4 : (a-e) Xray diffractograms of samples (1-5) respectively. Note two extra peaks for samples (1-4), that are not observed in diffractogram of sample (5).
- Figure 5: (a) A bright field TEM image showing inclusions of different sizes in sample (4). These inclusions are typical of those observed in samples (1-4).
- Figure 6 : Microdiffraction patterns from the inclusion shown in the image in Fig.5(a). The patterns are indexed as (a) $[110]_{fcc}$; (b) $[112]_{fcc}$ and (c) $[013]_{fcc}$. These micro-diffraction patterns were obtained with a nominal probe size of 400Å.
- Figure 7 : (a) Bright field TEM image showing the microanalytical line profile across the triple junction ; (b) a typical EDX spectrum from the grain boundary phase, showing the oxygen peak as well as the prominent Nd peak ; (c) EDX line profile data for the

region depicted in (a) ; (d) typical EDX spectrum from the inclusion obtained using an ultra-thin window EDX detector.

Figure 8 : (a) In-focus image showing two inclusions, from sample (4) ; (b), (c) and (d) show sequential Fresnel Lorentz images of a domain wall, as a function of the foil tilt. Note the strongly pinned configuration in (c).

Figure 9 : (a) In-focus image of an inclusion from sample (3) ; (b) spiked domain wall, pinned at the inclusion.

Figure 10 : Multiple domain walls observed around a large inclusion in sample (4).

Figure 11 : A plot of nucleation field against effective anisotropy field for the magnets with various amounts of Ho additions. Note that the slope of the linear fit is much larger than 0.38.

TABLE I
COMPOSITION OF ALLOYS STUDIED

SAMPLE NO.	PROCESSING	Wt.% Fe	Wt.% Nd	Wt.% Ho	Wt.%B
1.	Blending of master alloys	62.10	33.90	3.00	1.00
2.	Blending of master alloys	62.65	30.35	6.00	1.00
3.	Blending of master alloys	63.28	26.72	9.00	1.00
4.	Blending of master alloys	63.80	23.10	12.10	1.00
5.	Ho cast-in	63.80	23.10	12.10	1.00

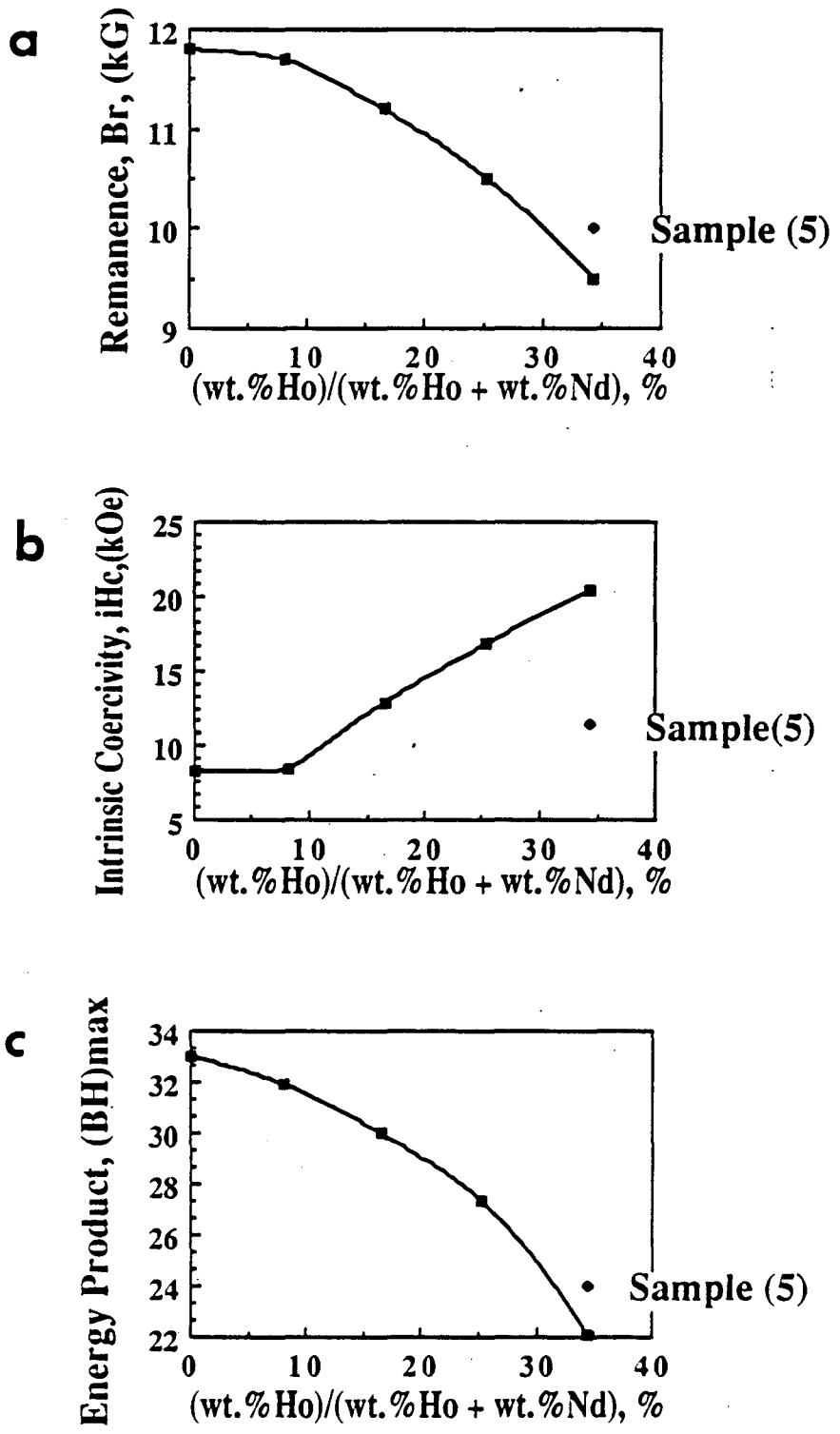
TABLE II
RATIO OF INTENSITY OF PEAKS AT 37° AND 53° TO THE 006_{matrix}

SAMPLE NO.	Ho CONTENT WT.%	PEAK	
		RELATIVE INTENSITY OF PEAK $\approx 37^\circ$	RELATIVE INTENSITY OF PEAK $\approx 53^\circ$
1.	3.0	6.1	4.0
2.	6.0	8.6	4.3
3.	9.0	13.5	9.5
4.	12.0	26.2	9.8
5.	12.0	0.0	0.0

* NOTE : The intensity of the two peaks are relative to that of the (006)_{matrix} peak, which is taken as 100% intensity.

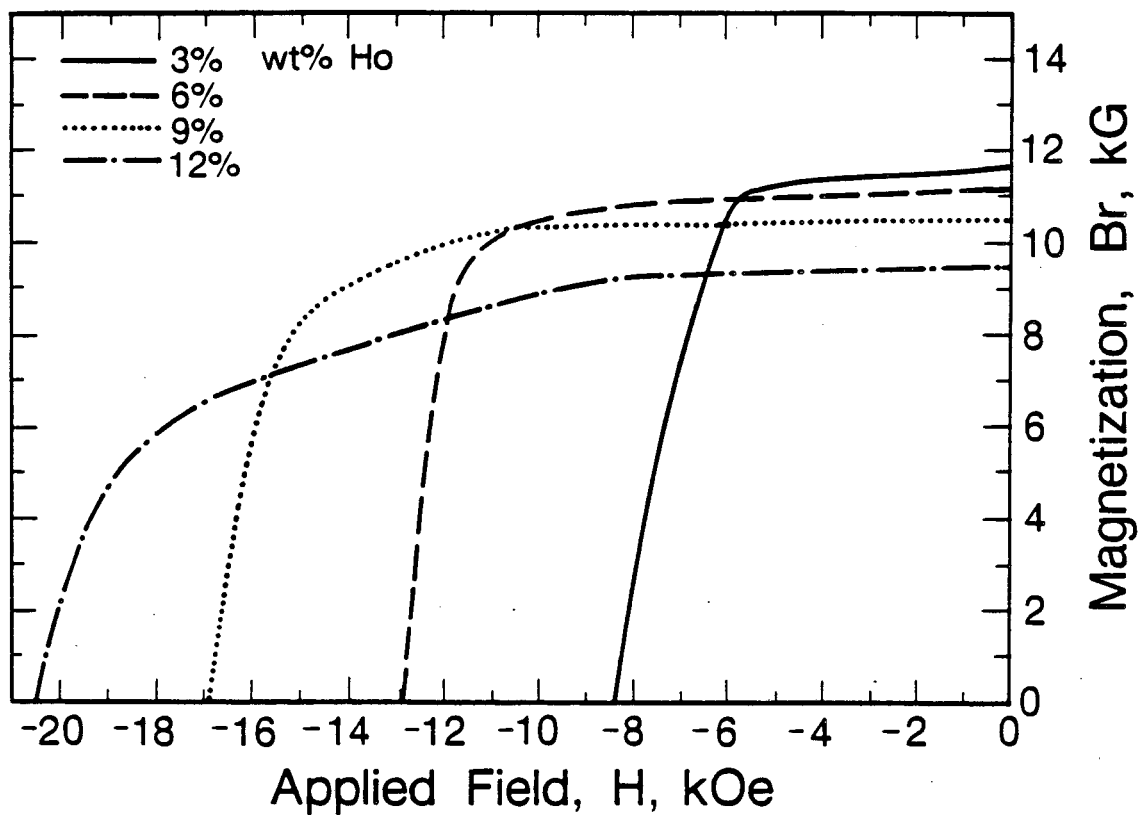
TABLE III
RESULTS OF ANALYTICAL ELECTRON MICROSCOPY POINT ANALYSES

SAMPLE NO.	PHASE REGION	At.% Fe	At.% Nd	At.%Ho	At.%O
4.	matrix	85.75	9.82	4.44	0.00
4.	fcc phase	6.89	60.29	0.76	32.04
4.	fcc inclusion	5.89	41.00	13.28	39.83
5.	matrix	86.35	9.12	4.53	0.00



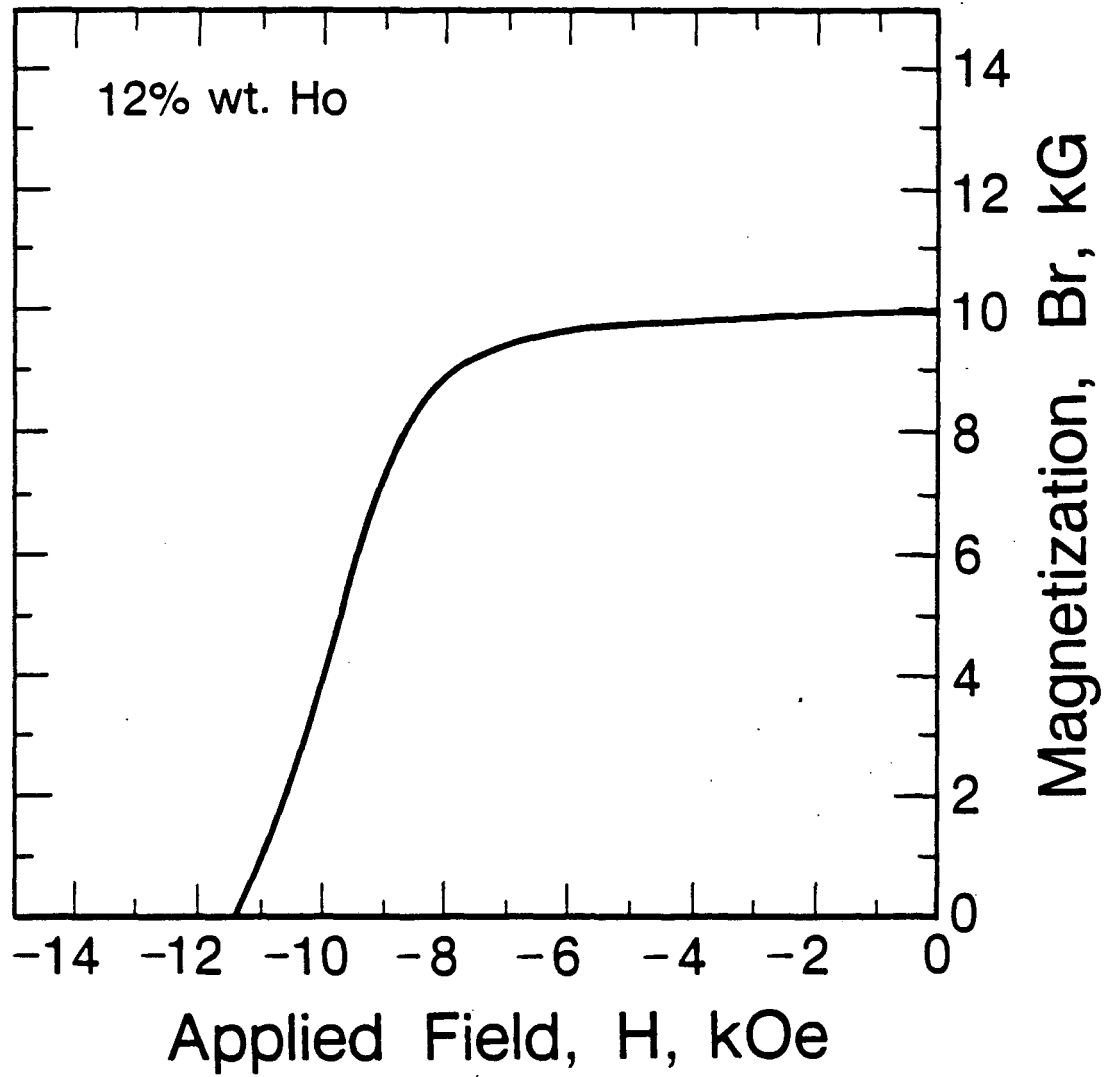
XBL 886-2363

Fig.I(a-c)



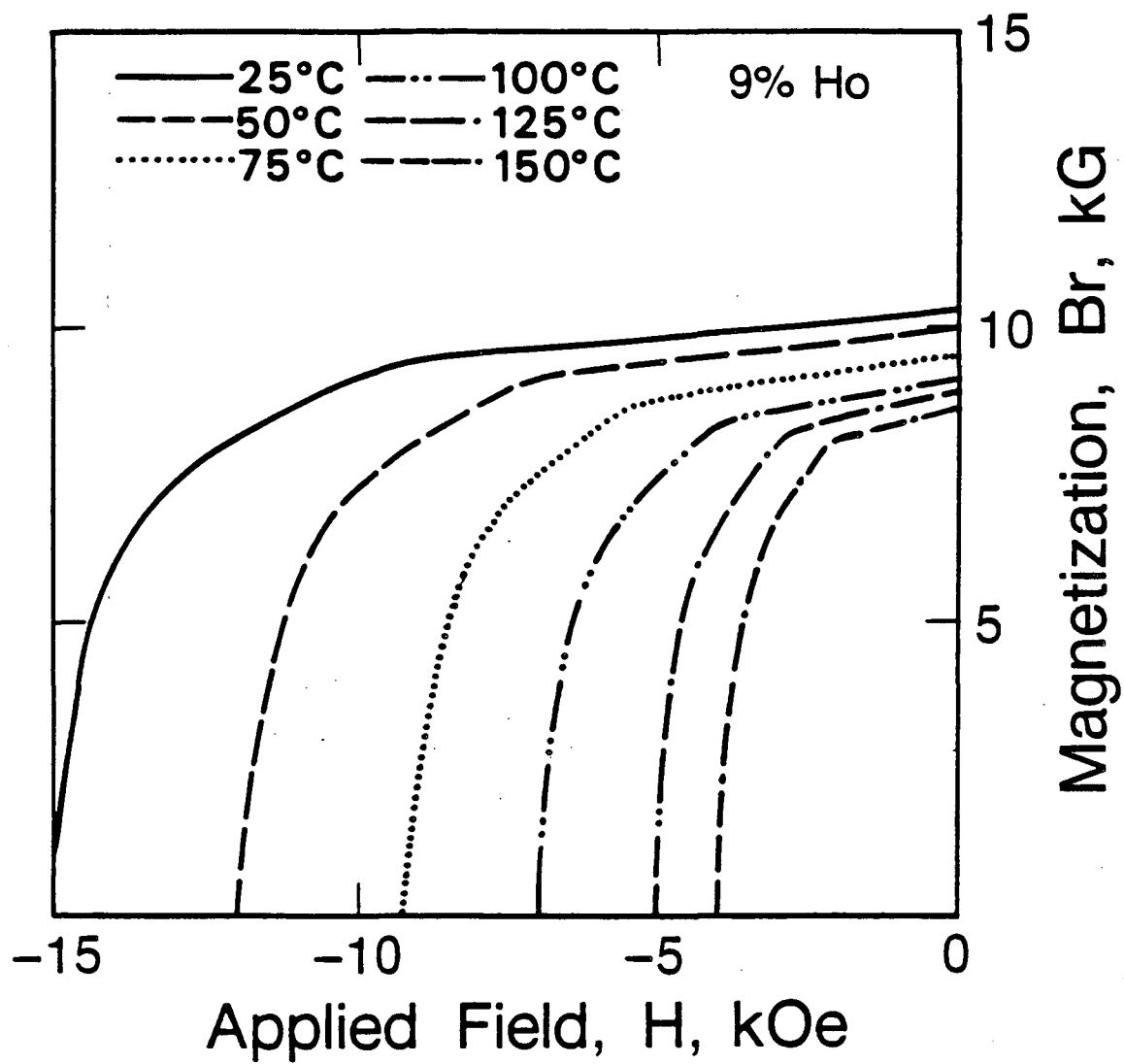
XBL 8711-7977

Fig.2(a)



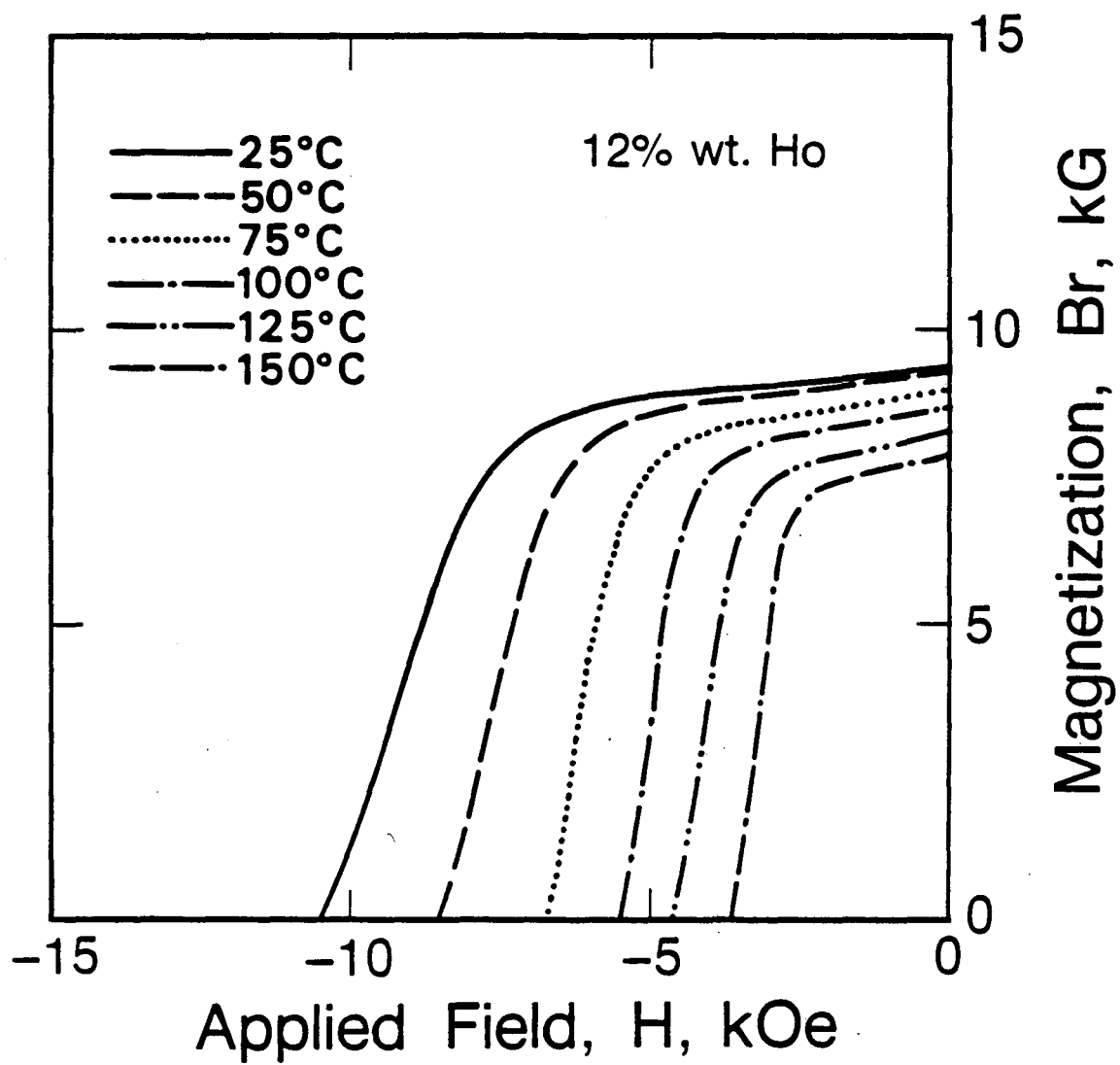
XBL 8710-7974

Fig.2(b)



XBL 8710-7966

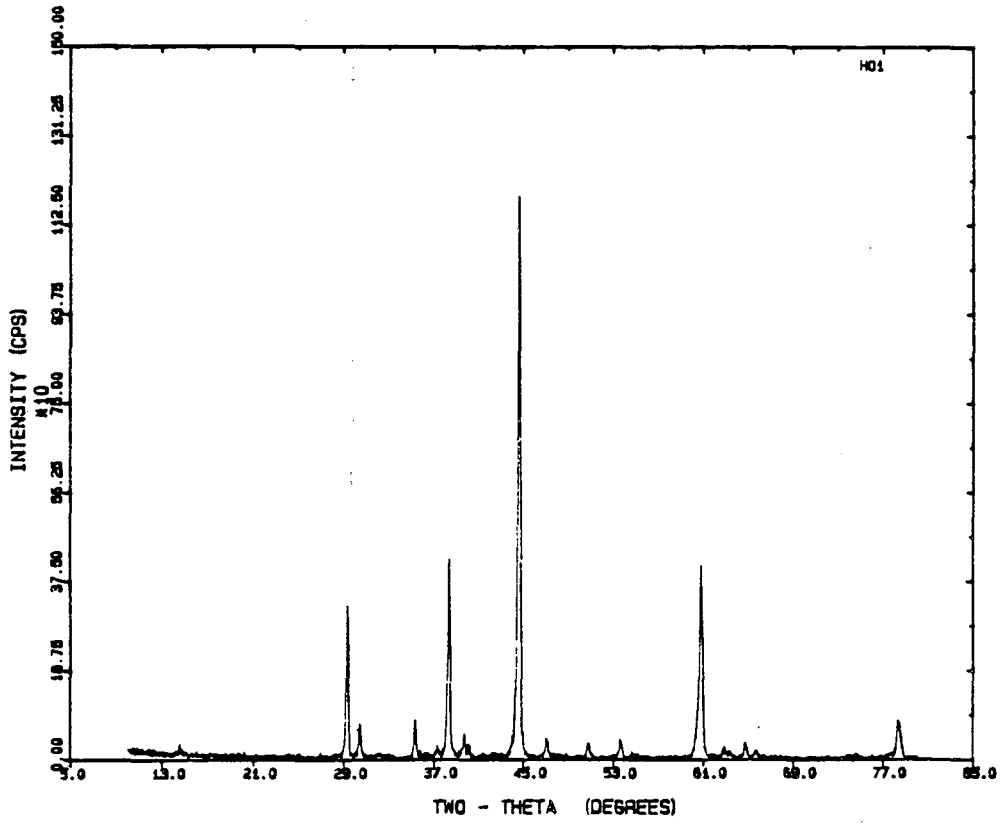
Fig.3(a)



XBL 8710-7973

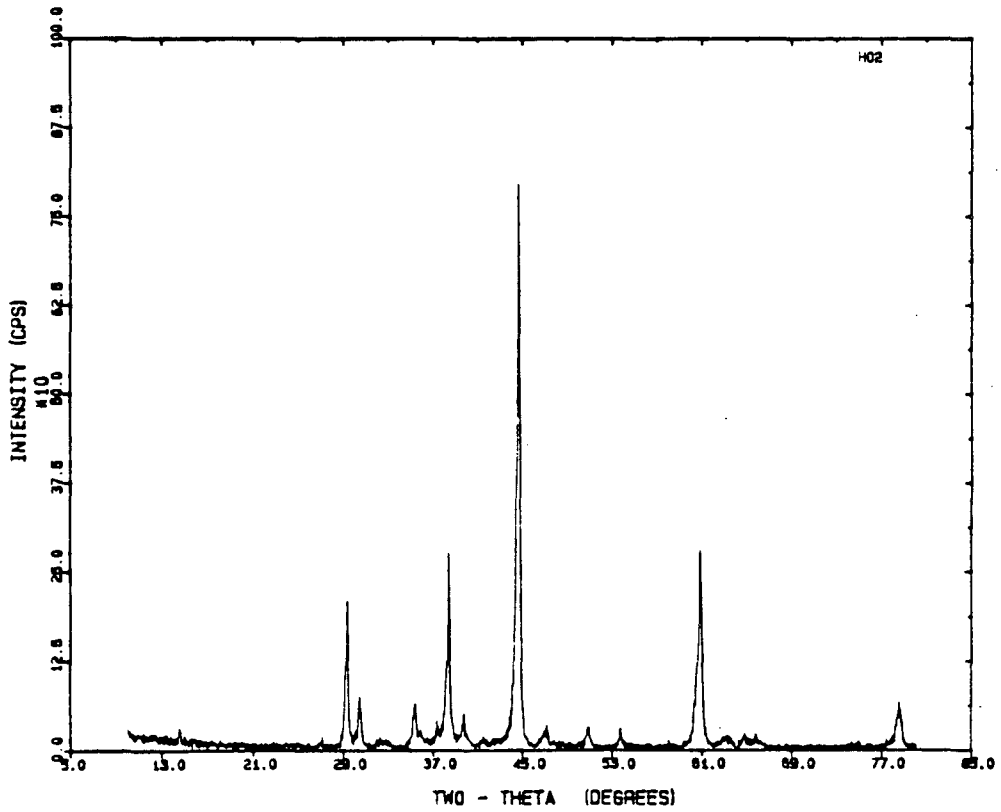
Fig.3(b)

a



XBL 877-3212

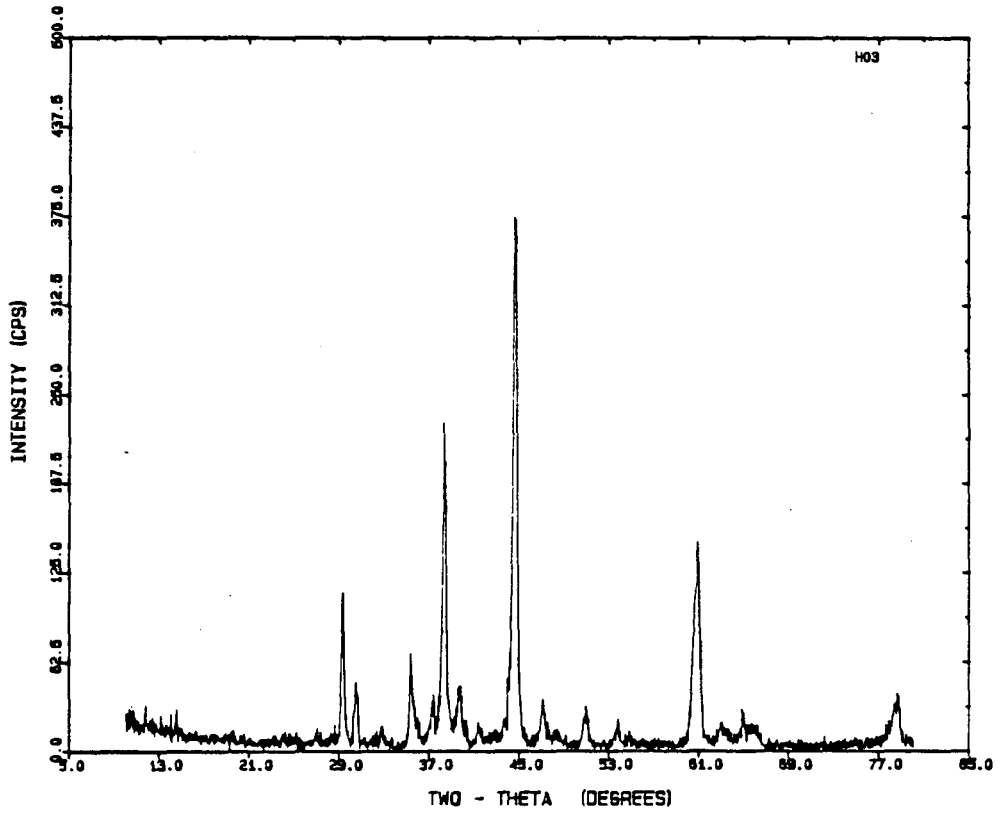
b



XBL 877-3214

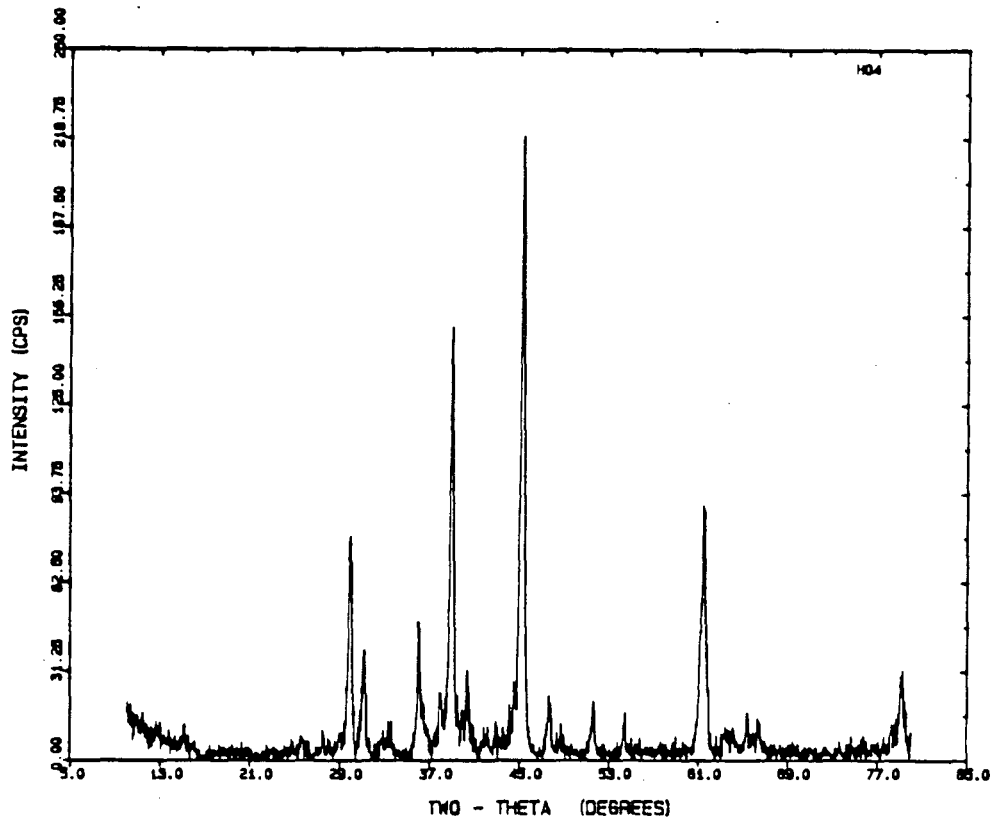
Fig.4(a,b)

c



XBL 877-3215

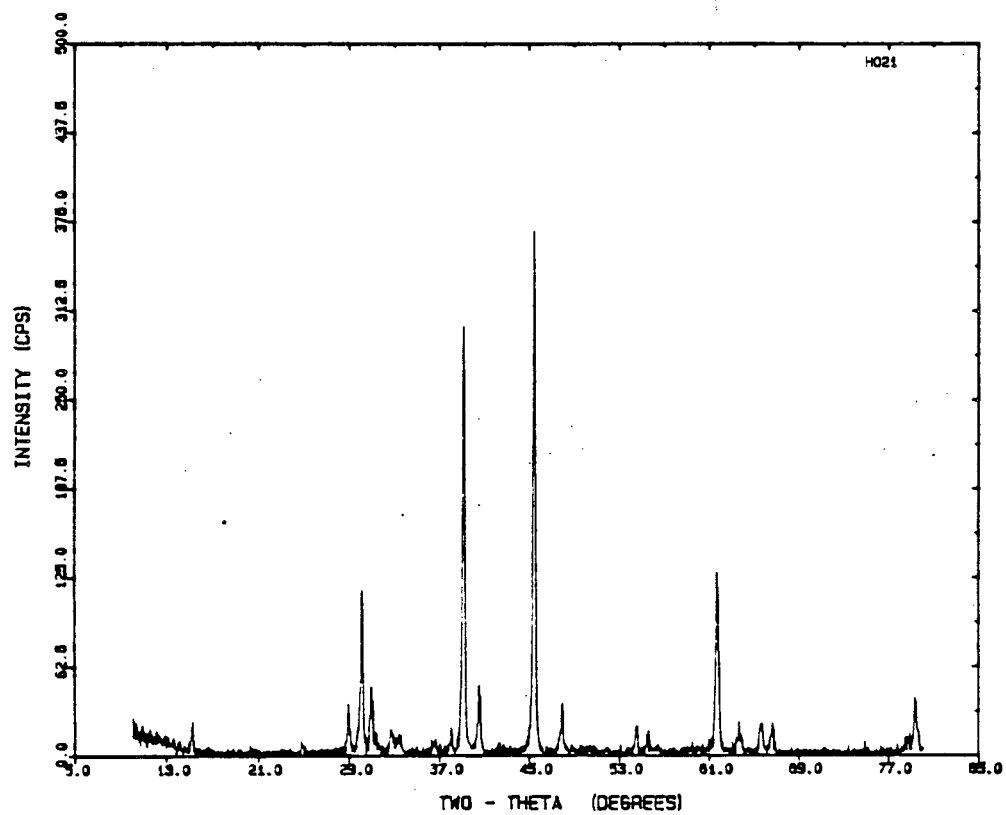
d



XBL 877-3216

Fig.4(c,d)

①



XBL 877-3213

Fig.4(e)

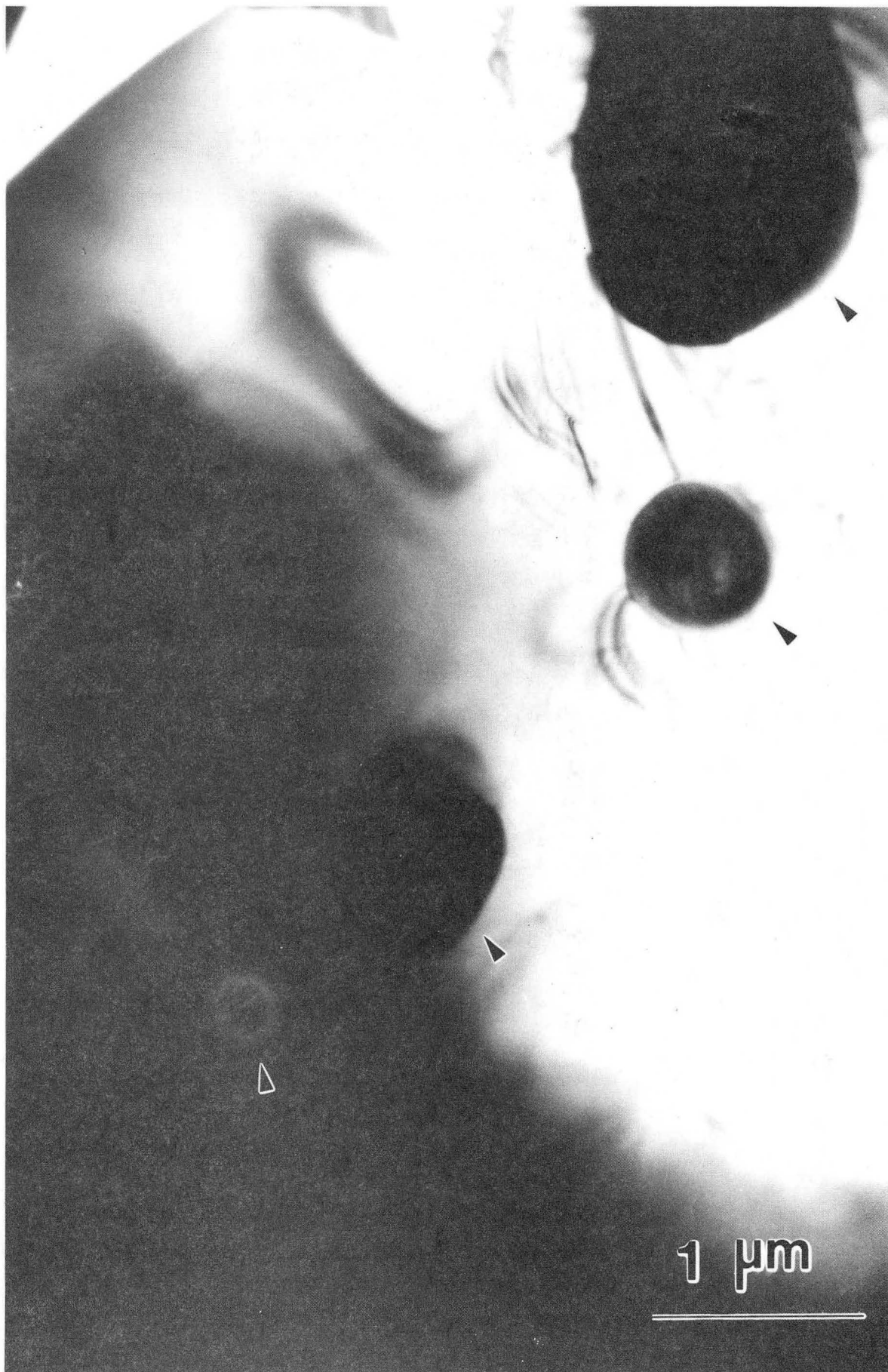
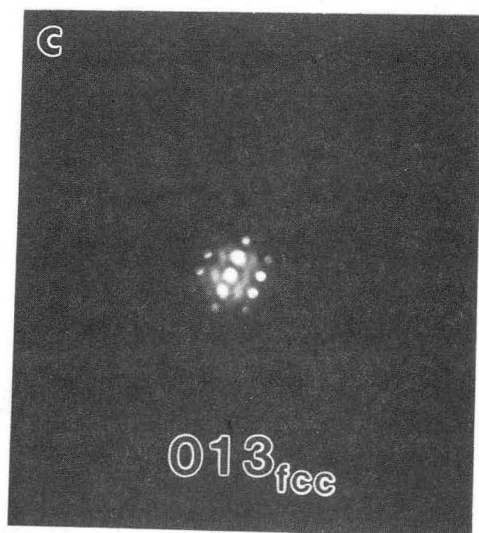
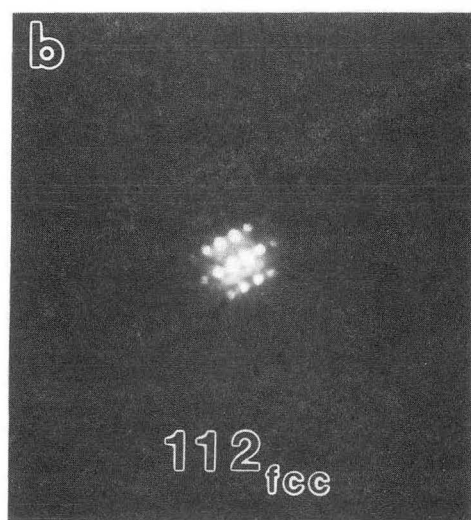
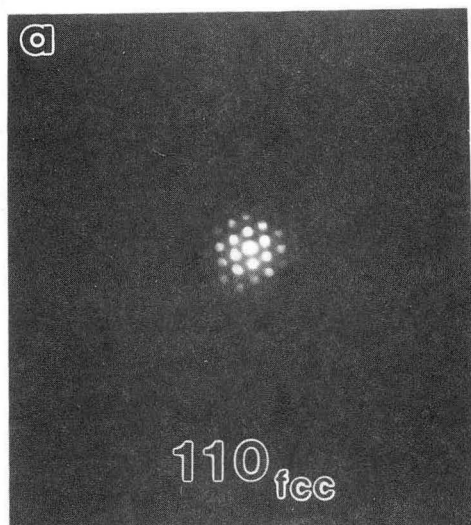


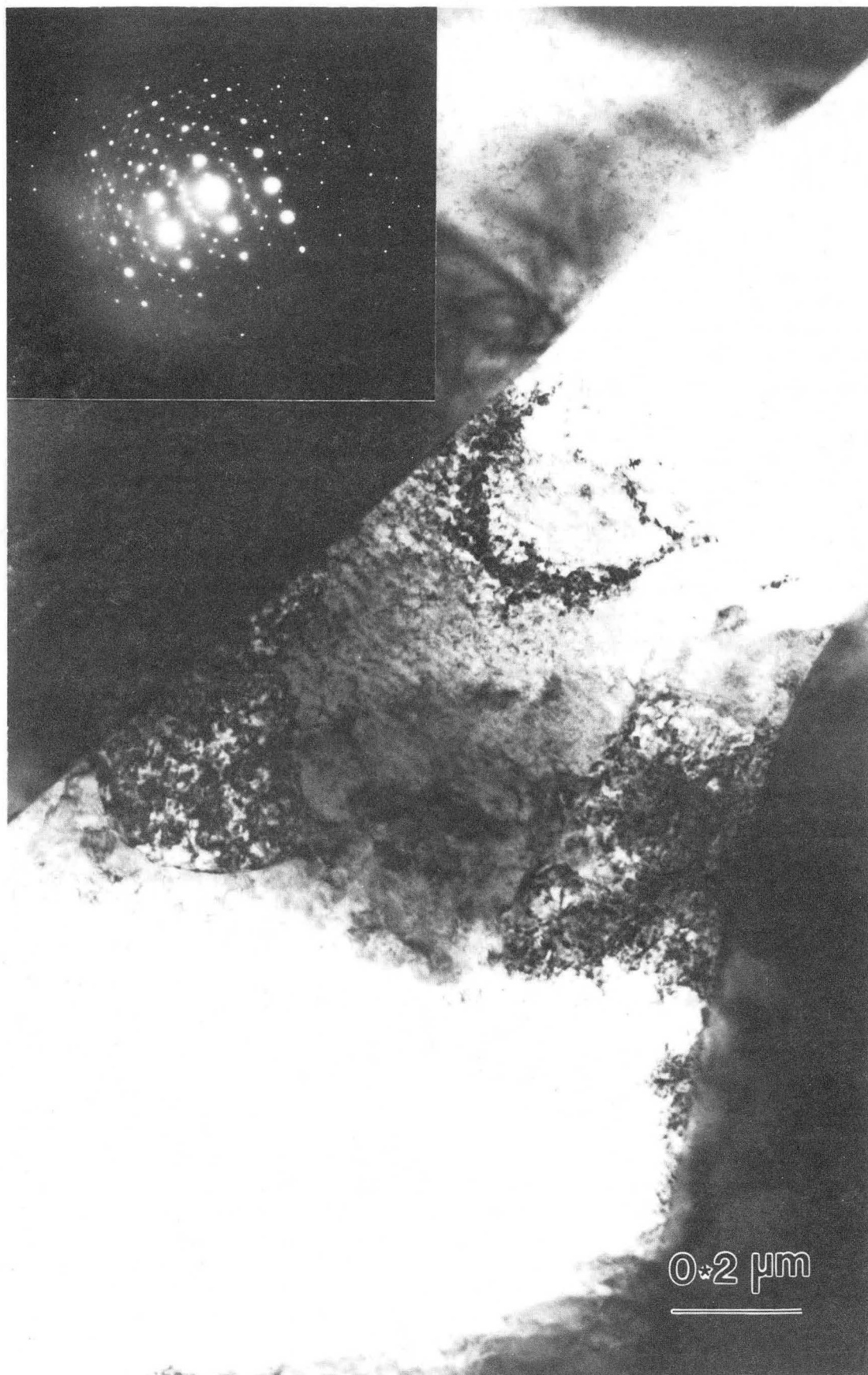
Fig.5

XBB 870-9959



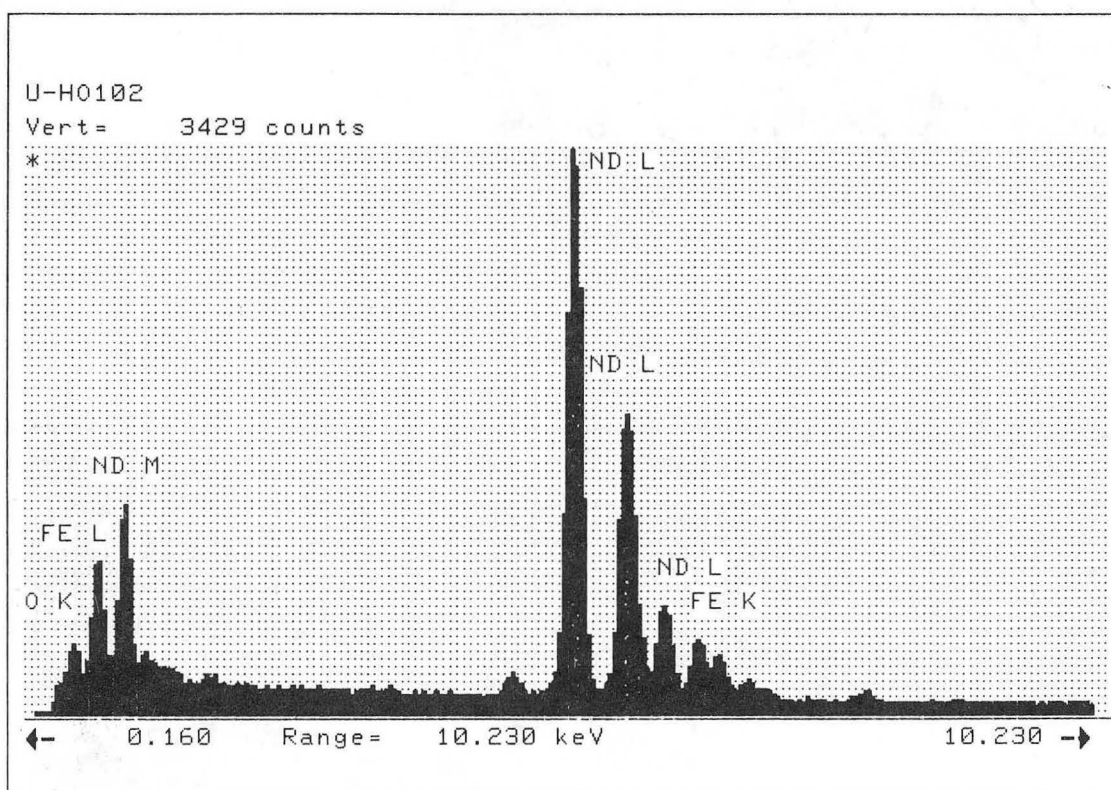
XBB 870-10328

Fig.6(a-c)



XBB 870-9961

Fig.7(a)



XBL 878-3537

Fig.7(b)

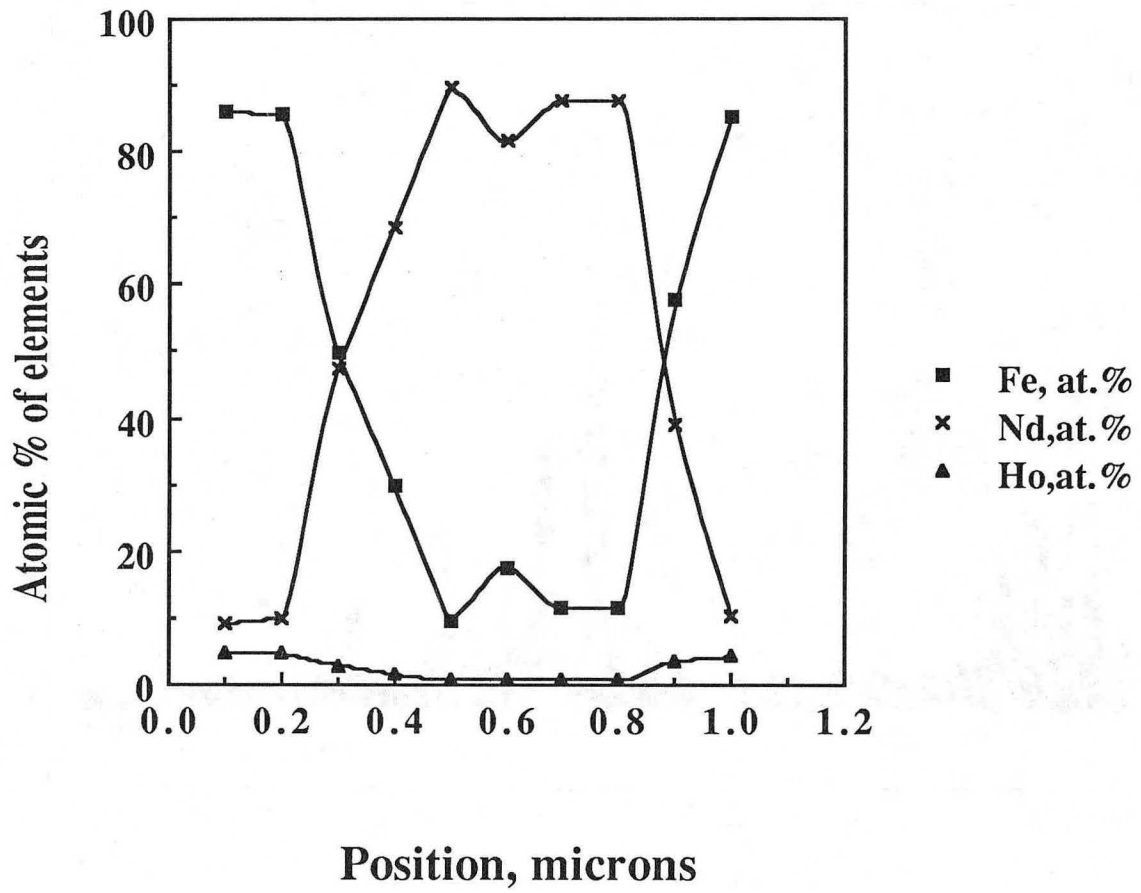
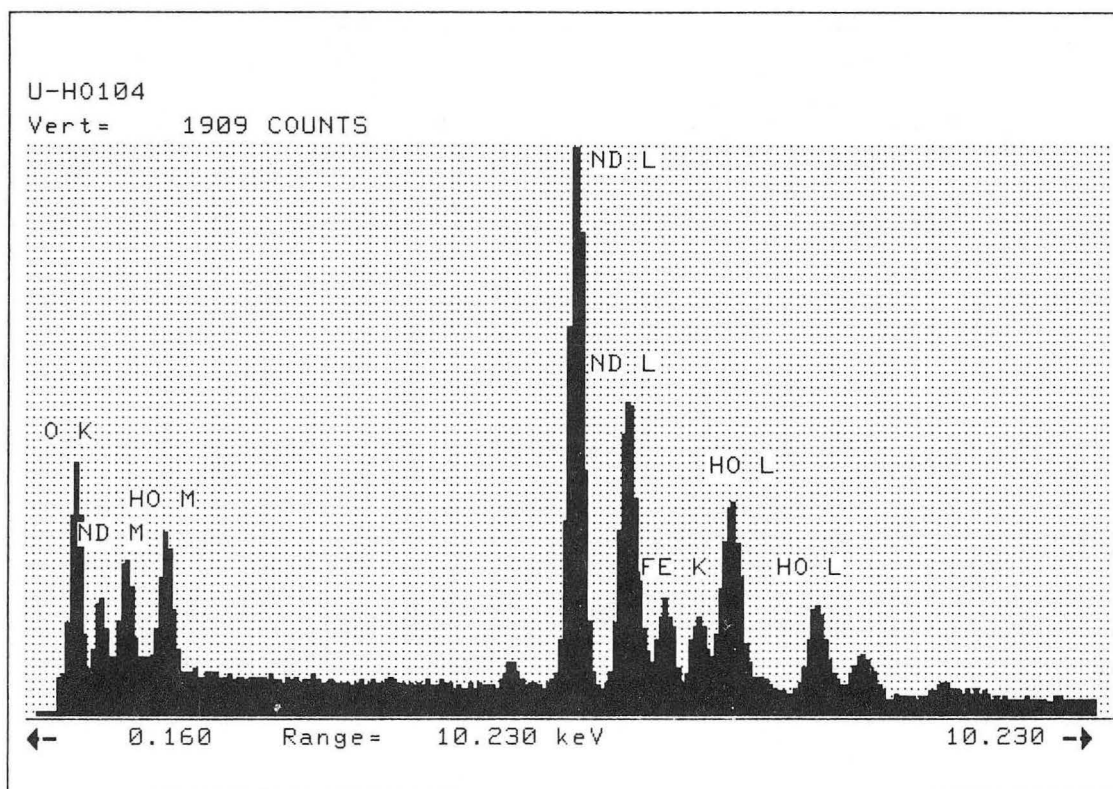


Fig.7(c)



XBL 878-3538

Fig.7(d)

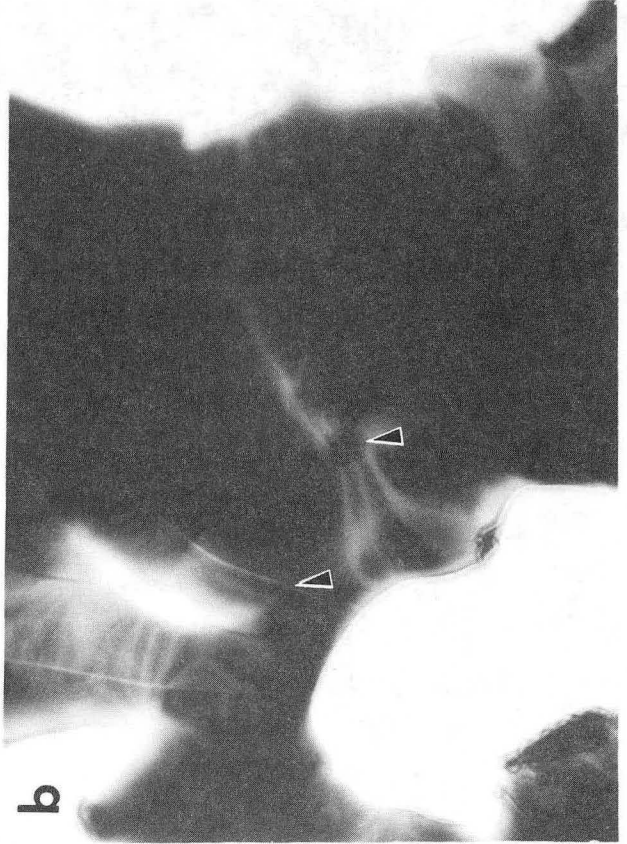
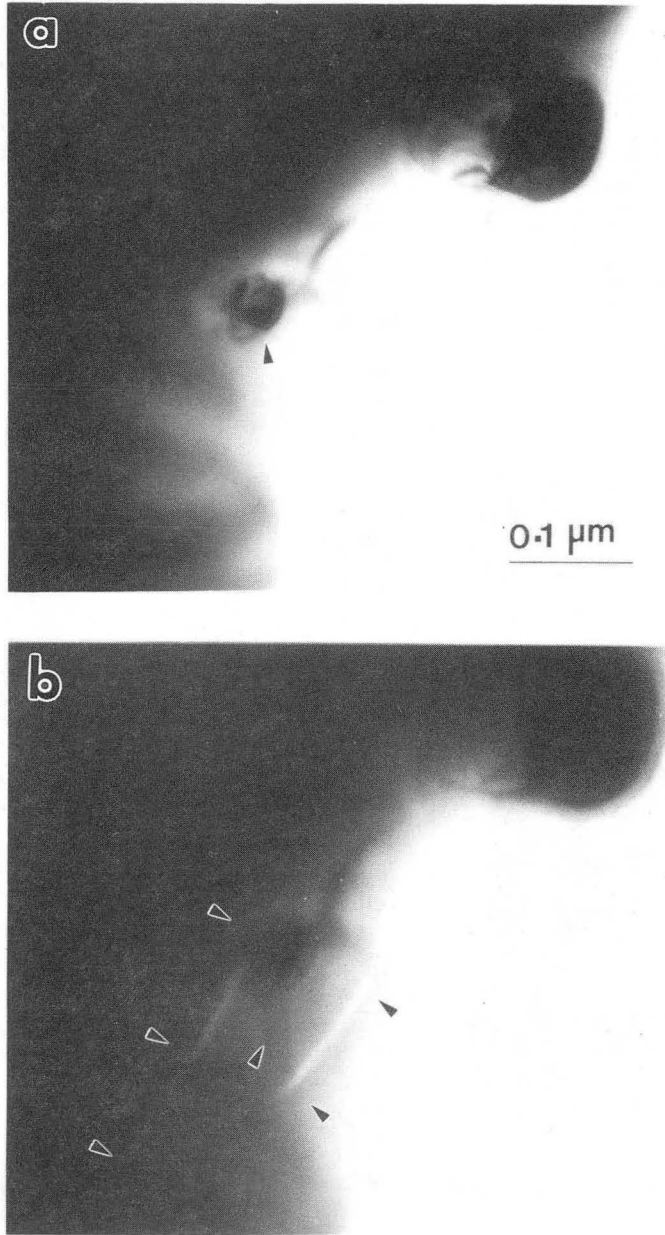


Fig. 8 (a-d)

XBB 878-6490



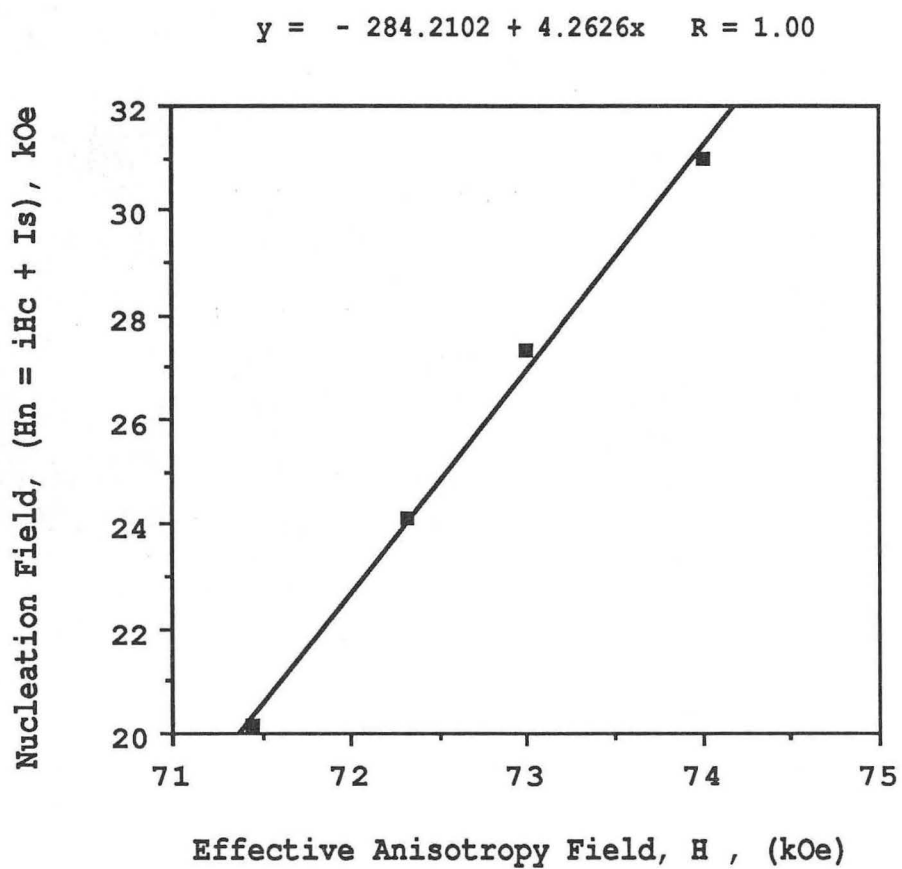
XBB 870-9956

Fig.9(a,b)



XBB 887-6765

Fig. 10



XBL 887-2393

Fig.II

*LAWRENCE BERKELEY LABORATORY
TECHNICAL INFORMATION DEPARTMENT
UNIVERSITY OF CALIFORNIA
BERKELEY, CALIFORNIA 94720*